International Journal of Solids and Structures 45 (2008) 4247–4263

Contents lists available at ScienceDirect

International Journal of Solids and Structures

journal homepage: www.elsevier.com/locate/ijsolstr

Use of a modified torsional Kolsky bar to study frictional slip resistance in rock-analog materials at coseismic slip rates

Fuping Yuan, Vikas Prakash *

Department of Mechanical and Aerospace Engineering, Case Western Reserve University, Cleveland, OH 44106-7222, USA

A R T I C L E   I N F O

Article history:
Received 25 October 2007
Received in revised form 23 February 2008
Available online 21 March 2008

Keywords:
Rock mechanics
Torsional Kolsky bar
Slip Weakening
Glass-on-glass
Slip strengthening
Coseismic slip velocity

A B S T R A C T

The knowledge of shear resistance in earth faults is of fundamental importance to our understanding of the magnitude of stress drop and the associated energy release during typical seismic rupture events. In the present study a modified torsional Kolsky bar is employed to investigate frictional slip resistance in rock-analog materials (i.e., quartz and soda lime glass) at normal stresses of relevance to earthquake physics (30–80 MPa) and co-seismic slip rates. The results indicate the coefficient of kinetic friction to be in the range of 0.2 to 0.3. These values of the coefficient of friction are much lower when compared to those obtained in rocks at quasi-static slip rates. In all experiments slip weakening is observed and is preceded by slip strengthening. The slip weakening is understood to be due to thermal weakening induced by flash-heating at asperity contacts and requires a few mm of slip to be effective; the slip strengthening is understood to be due to an increase in the real area of contact at the asperity junctions due to localized plastic flow and subsequent coalescence and solidification of local softened/melt patches at the slip interface.

1. Introduction

Knowledge of shear resistance in earth faults during earthquakes is fundamental information for understanding earthquake physics and energy released during such events. Friction resistance at constant normal stress and sliding speeds of less than 1 mm/s have been well studied for a wide range of geo-materials. The characterization of these results in terms of rate and state variable friction laws has allowed a much better understanding of a wide variety of aspects of the mechanics of earthquakes (Scholz et al., 1972; Dieterich, 1979, 1981; Rice and Ruina, 1983; Ruina, 1983; Dieterich and Kilgore, 1994; Tullis, 1994; Dieterich and Kilgore, 1996b; Blanpied et al., 1998; Marone, 1998; Scholz, 1998; Di Toro et al., 2004), including, for example, what to expect in terms of premonitory slip and Omori's Law for aftershock decay (Scholz, 1998).

Experimental data suggest that frictional resistance in rock and rock-analog-materials at slip speeds <1 mm/s and slip distance <1 mm is in the range of 0.6 to 0.85 (Byerlee, 1978; Dieterich, 1978; Dieterich and Kilgore, 1996a). However, seismic inversions provide evidence that frictional resistance of major faults at co-seismic slip speeds (1–2 m/s) may be quite low (Heaton, 1990; Rice, 2006). Moreover, very little data exist for the simultaneously high slip rates and large slip displacements characteristic of co-seismic slip, and the data that do exist suggest that the frictional behavior at these slip speeds is dramatically different and the dynamic slip weakening occurs (Sibson, 1973; Tsutsumi and Shimamoto, 1997; Goldsby and Tullis, 2002; Di Toro et al., 2004; Mizoguchi et al., 2006; O'Hara et al., 2006).

Rudnicki and Rice (2006), Segall and Rice (2006), Rempel and Rice (2006) and Rice (2006) have recently summarized two primary thermal weakening mechanisms which are assumed to act in combination during fault events: (1) flash heat-

* Corresponding author. Tel.: +1 216 368 6440; fax: +1 216 368 3007.
E-mail address: vikas.prakash@case.edu (V. Prakash).

0020-7683/$ - see front matter © 2008 Elsevier Ltd. All rights reserved.
doi:10.1016/j.ijsolstr.2008.03.012

ing and consequent weakening at highly stressed asperity contacts during rapid slip which reduces the friction coefficient, a phenomenon studied for many years as the key of understanding the slip rate dependence of dry friction in metals at high slip rates (Bowden and Thomas, 1954; Archard, 1958; Barber, 1976; Kuhlmann-Wilsdorf, 1985; Ashby et al., 1991; Irfan and Prakash, 1994), and which has also been considered recently in seismology as a mechanism that could be active in controlling fault friction during seismic slip before macroscopic melting (see also Andrews, 2002; Hirose and Shimamoto, 2005; Wibberley and Shimamoto, 2005); and (2) thermal pressurization of pore fluid within the fault core by frictional heating which assumes the presence of water within shallow crustal fault zones such that the effective normal stress $\bar{\sigma}_n$ ($\bar{\sigma}_n = \sigma_n - p$, where σ_n is the compressive normal stress on the fault, and p is the pore fluid pressure) controls the frictional strength, and which reduces the effective normal stress and hence the shear resistance associated with any given friction coefficient (Sibson, 1973; Lachenbruch, 1980; Mase and Smith, 1985; Lee and Delaney, 1987; Mase and Smith, 1987; Andrews, 2002; Wibberley, 2002; Noda and Shimamoto, 2005; Sulem et al., 2005). Under the right conditions, these two mechanisms are understood to become important immediately after seismic slip initiates (Segall and Rice, 2006).

In an attempt to investigate the first of the two aforementioned weakening mechanisms, Hirose and Shimamoto, 2005) conducted a series of experiments on Indian gabbro at slip rates of 0.85–1.49 m/s and normal stresses of 1.2–2.4 MPa using a rotary-shear apparatus. The experiments on gabbro revealed two stages of slip weakening separated by a marked strengthening regime. By examination of microstructures of simulated fault zone under scanning electron microscopy (SEM) at different total slip displacements, they proposed that the initial slip weakening is due to the thermal weakening induced by flash heating at the asperity contacts and early stages of melting; this phase is followed by slip strengthening caused by the coalescence of melt patches into a thin molten layer; while the second slip weakening is attributed to the growth of molten layer during friction melting. Another weakening mechanism, i.e., by the formation of silica gel, has been identified by Di Toro et al. (2004). They studied the slip resistance of Arkansas Novaculite rock at a slip rate of 0.03 m/s and a normal stress of 5 MPa using a servo-controlled compression-torsion apparatus. They attributed the initial slip weakening mechanism to the formation of silica gel, and the time-dependent recovery of shear strength to the thixotropic behavior of the silica gel. Although different physical processes, such as, flash heating at asperity contacts, formation of silica gel, and frictional melting have been proposed that could lower shear resistance during fast co-seismic slip, these mechanisms and/or their applicability to earthquakes are still poorly understood.

In the present study, a series of experiments are conducted to investigate frictional resistance in rock-analog materials such as quartz and soda-lime glass at co-seismic slip rates by using a modified torsional Kolsky bar (Rajagopalan et al., 1999; Rajagopalan and Prakash, 1999). The objective of these experiments is to investigate the frictional resistance of relevant rock and analog materials at co-seismic slip speeds, so as to better understand the role of high slip speeds in leading to slip weakening at the slip interface by the mechanism of asperity flash heating and associated thermal softening with slip. The modified torsional Kolsky bar friction experiments are also expected to bridge the gap between the low slip-speed friction experiments (<1 mm/s) and the higher slip-speed plate-impact friction experiments ($\sim$20 m/s) reported by Yuan and Prakash (2008). Moreover, the results of this study have the advantage in making laboratory rock friction studies relevant not just to mechanisms of dynamic fault weakening but also to the constitutive description of the behavior that can be used in dynamic models for earthquake rupture.

2. Modified torsional Kolsky bar friction experiment

In the present study, a series of modified torsional Kolsky bar friction experiments were conducted on rock-analog material (quartz and soda-lime glass) samples. The choice of quartz and soda-lime glass as an analog material was dictated by a number of previous studies (Weeks et al., 1991; Dieterich and Kilgore, 1994, 1996a), which have shown that the frictional behavior of glass is almost identical to that of rocks. Details of the modified torsional Kolsky bar friction experimental configuration and specimen preparation are provided next.

2.1. Experimental configuration

The schematic of the modified torsional Kolsky bar apparatus is shown in Fig. 1. In this setup, a thin-walled tubular specimen is mounted at the end of the solid incident bar, while the transmitter bar of the conventional torsional Kolsky bar is replaced by a quartz or soda-lime glass disk connected to a rigid support. Besides providing a rigid boundary condition, the disk also represents the other half of the tribo-pair. In order to conduct the experiments, the specimen on the incident bar is made to slide axially in the alignment fixture by applying a static axial compressive force of pre-determined magnitude by employing a hydraulic actuator at the pulley end of the modified torsional Kolsky bar apparatus until it makes contact with the disk on the rigid support. An important consideration in the implementation of the experiment is that the sliding face of the tubular specimen should remain parallel and in contact with the other face representing the tribo-pair, at all times during the sliding process. This is achieved by using an alignment fixture, schematically illustrated in Fig. 2, which ensures that the tubular specimen is aligned perpendicular to the other surface of the tribo-pair, i.e., the surfaces in contact – which are lapped flat prior to the experiment – are parallel to each other, at all times. The alignment fixture has a Teflon bearing which allows free rotation in either direction as well as normal motion.

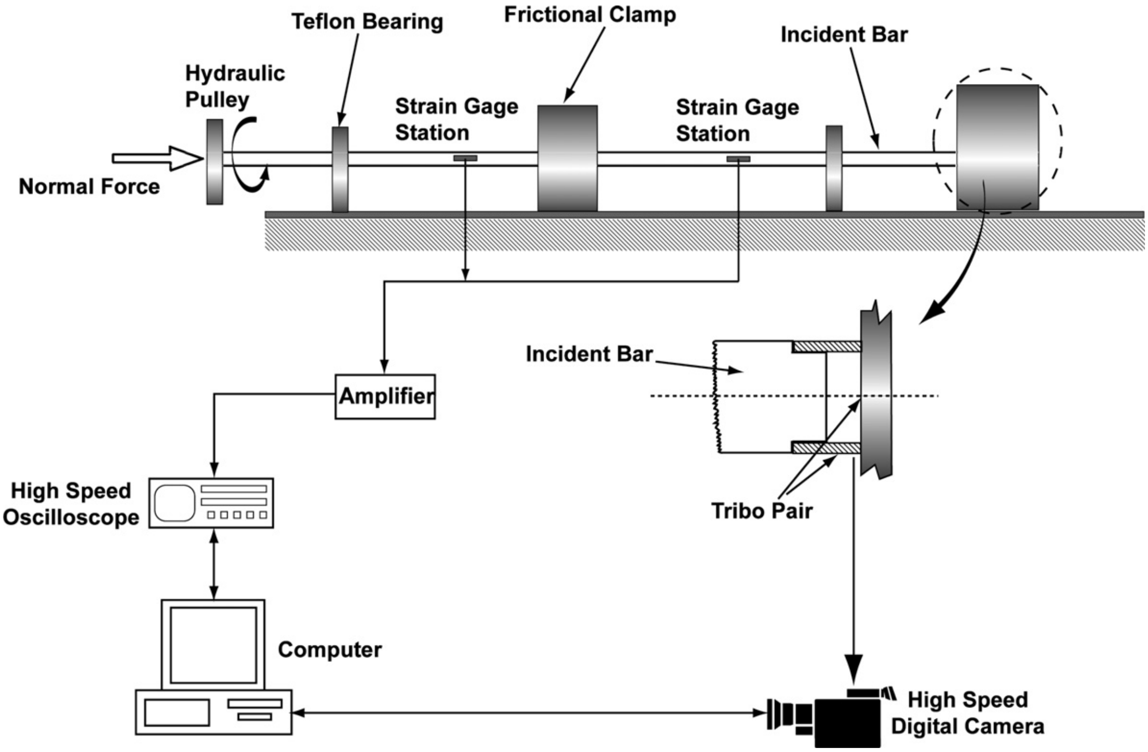

Fig. 1. Schematic of the modified torsional Kolsky bar friction experiment. The Al 7075-T6 solid bar is 25.4 mm diameter and 4 m in length. The distance between the pulley system and frictional clamp is 1.67 m.

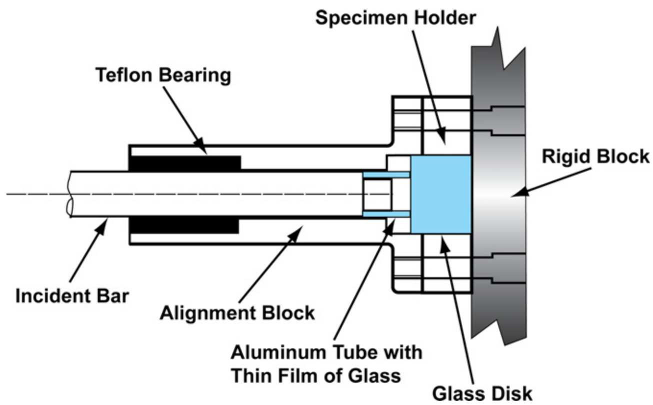

Fig. 2. Alignment fixture to ensure parallelism of the tribo-pair surfaces. The tubular specimen is 25.4 mm in diameter, 12.5 mm in length, and has a wall thickness of about 3 mm; the disk specimen is 37 mm in diameter and 12.5 mm in length.

Next, a torsional loading pulse is generated by a sudden release of stored torque. This requires a torque pulley system at the end of the incident bar and a frictional clamp positioned a short distance from the pulley end. The torque is generated by employing a hydraulic actuator to twist the pulley attached to the end of the incident bar. The frictional clamp allows the desired torque to be held without slipping and releases the torque rapidly enough – when the pre-notched pin breaks – to release to a sharp fronted stress pulse which travels towards the tribo-pair specimens. During the experiment the input and the reflected torsional pulses from the tribo-pair interface are measured by strain gages attached to the surface of the incident bar. Moreover, an ultra-high-speed digital camera (Imacon 200, DRS Technologies) is employed to monitor the slip interface during the experiment. Other details regarding the design, execution and data analysis of the experiments can be found in Rajagopalan and Prakash (1999) and Rajagopalan et al. (1999).

In order to conduct the glass-on-glass friction experiments either a thin-walled quartz tube or a thin-walled aluminum tube with a thin film of soda lime glass ($\sim$1 μm thickness) deposited on one of its faces (by using a vapor deposition procedure at the Electronics Design Center (EDC), CWRU), is used as one-half of the tribo-pair. A quartz disk or a soda-lime glass disk (connected to a rigid support) is used as the other half of the tribo-pair.

2.2. Wave analysis: calculation of interfacial tractions, slip velocity, slip distance

The wave propagation diagram for the modified torsional Kolsky bar apparatus is illustrated in Fig. 3. Position of the wave front versus time is detailed. The duration of the loading pulse is the time required for the pulse to travel twice the distance between the pulley and the frictional clamp. The time $t = 0$ corresponds to the time at which the frictional clutch is released. At this instant the state in the solid bar to the left of the frictional clamp is equal to the applied torque T_0 and zero angular velocity. The solid bar to the right of the clamp has zero torque and zero angular velocity. When the clamp is released half of the input torque propagates as a torsional pulse to the left and the other half propagates to the right in the solid bar towards the tribo-pair interface. Upon the release of the clamp the state is given by 1. The reflected wave from the pulley end travels towards the clamp unloading the bar to state 3 which corresponds to a completely unloaded state. The strain gage at station A sees state 1 until the wave reflected from the pulley end of the solid bar returns to the gage station and results in state 3. The wave reflected from the tribo-pair interface returns to gage station A and results in state 5. This returning wave carries information of the frictional state at the tribo-pair interface. By measuring the torsional strain on the incident bar at gage location A, the critical interfacial frictional parameters at the tribo-pair interface such as the frictional stress, the interfacial slip speed and the accumulated slip displacement can be interpreted using the framework of one-dimensional plane-wave analysis.

For the case in which there is full sticking at the tribo-pair interface the state of frictional interface is represented by point A in Fig. 4. For the other extreme case, i.e., when the tribo-pair interface can support zero frictional stress, the angular velocity at the frictional interface is represented by the point B. For any other case in between, i.e., when the torque supported by the tribo-pair interface is given by $T_{\text{interface}}$, the corresponding angular slip speed at the frictional interface is given by

$$\omega_{\text{interface}} = \frac{(T_{\text{interface}} - 2T_1)}{(\rho CJ)_{\text{tube}}}, \tag{1}$$

where T_1 is the known input torque at the tribo-pair interfaces.

In order to obtain the frictional torque at the tribo-pair interface, $T_{\text{interface}}$, a backward drawn characteristic joining the states ($T_{\text{interface}}$, $\omega_{\text{interface}}$) and ($T_5$, ω_5), and a forward drawn characteristic joining the states (T_3, ω_3) and (T_5, ω_5), are used. Moreover, using the fact that state 3 is a zero state the torque at the tribo-pair interface can be expressed in terms of the measured torques T_1 and T_5, i.e.,

$$T_{\text{interface}} = T_1 + T_5, \tag{2}$$

and

$$\omega_{\text{interface}} = \frac{(T_{\text{interface}} - 2T_1)}{(\rho CJ)_{\text{bar}}}. \tag{3}$$

Once the interfacial torque and the interfacial angular slip speed are obtained, the average interfacial friction stress and the average interfacial slip speeds at the tribo-pair interface can be obtained using

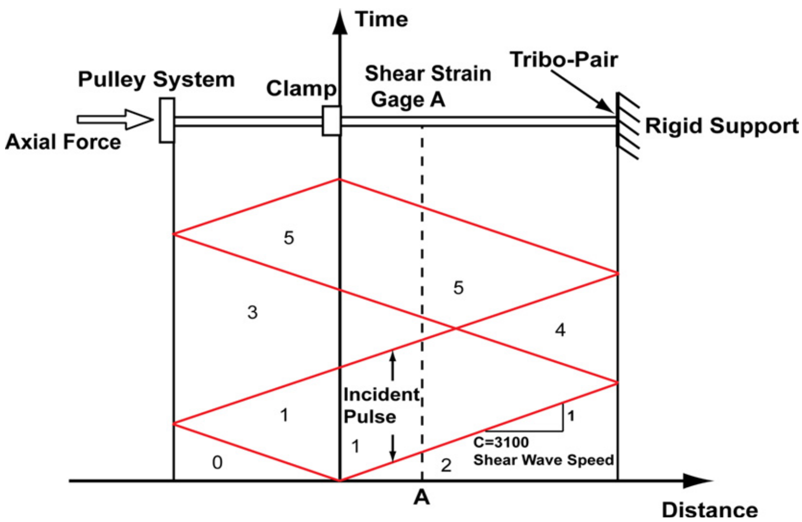

Fig. 3. Wave propagation diagram for the modified torsional Kolsky bar. Position of the wavefronts versus time are detailed.

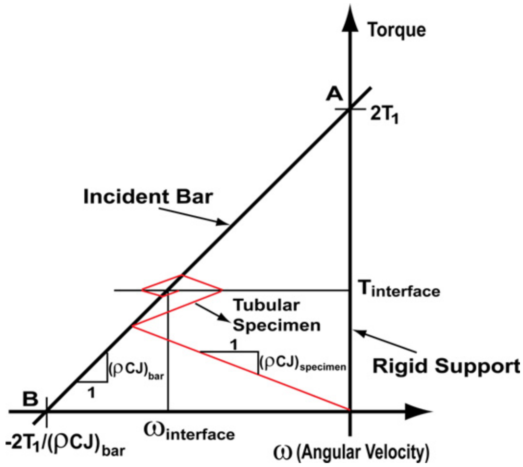

Fig. 4. Loci of all the torque and angular velocity states that can be attained at the tribo-pair interface.

$$\tau_{\text{interface}}(t) = \frac{\int_{r_i}^{r_o} \tau(r,t) r \mathrm{d}r}{\int_{r_i}^{r_o} r \mathrm{d}r}, \quad \text{where } \tau(r,t) = r\frac{T_{\text{interface}}(t)}{J_{\text{specimen}}}, \tag{4}$$

and

$$V_{\text{slip}}(t) = \frac{\int_{r_i}^{r_0} \omega_{\text{interface}}(t) r^2 \mathrm{d}r}{\int_{r_i}^{r_0} r \mathrm{d}r}. \tag{5}$$

In Eqs. (4) and (5), r_i and r_o are the inner and outer radii of the thin walled tubular specimen, respectively.

The normal stress at the interface can be obtained from the measured axial strain in the incident bar, i.e.,

$$\sigma_{\text{interface}} = E\varepsilon_{\text{bar}} \frac{A_{\text{bar}}}{A_{\text{specimen}}}, \tag{6}$$

where E is the elastic modulus of the incident bar, and ε_{bar} is the measured axial strain in the bar.

The accumulated slip distance can be evaluated by integrating the slip velocity history, i.e.,

$$\delta_{\text{slip}}(t) = \int_0^t V_{\text{slip}}(t) \mathrm{d}t. \tag{7}$$

Then, by using the interfacial shear stress (Eq. (4)), and normal stress (Eq. (6)), the coefficient of kinetic friction μ_k can be obtained. i.e.,

$$\mu_k(t) = \frac{\tau_{\text{interface}}(t)}{\sigma_{\text{interface}}}. \tag{8}$$

2.3. Calculation of interfacial temperature rise

2.3.1. Temperature distribution as a function of distance from the sliding interface in the tubular specimen

By neglecting radiation and convection effects (since the thermal conductivity of soda-lime glass and/or quartz (see Table 1) are much larger than that of air ~0.024 W/m.k), the heat conduction in the tubular specimen is governed by the 1-D heat equation in a semi-infinite solid, i.e.,

$$\frac{\partial^2 T}{\partial x^2} = \frac{1}{\alpha}\frac{\partial T}{\partial t}, \tag{9}$$

with the initial condition

$$T(x,0) = 0, \tag{10}$$

Table 1
Summary of thermal properties of soda-lime glass and quartz

Materials	Thermal Conductivity k, (W/m.K)	Thermal diffusivity α, m^2/s
Soda-lime glass	1.38	0.891×10^{-6}
Quartz	5.46	1.84×10^{-6}

and the boundary conditions

$$-k\frac{\partial T}{\partial x}(x=0,t)=\dot{q}(t), \tag{11}$$

$$T(x=\infty,t)=0. \tag{12}$$

In Eqs. (9)–(12) T is the temperature rise, k is the thermal conductivity, α is the thermal diffusivity, and $\dot{q}(t)$ is heat source at $x = 0$, where x represents the perpendicular distance from the sliding interface.

By solving Eqs. (9)–(12) in the semi-infinite solid, the temperature rise distribution in the thin walled tube as a function of time and position can be expressed as

$$T(x,t)=\frac{1}{k}\int_0^t \dot{q}(\xi)\frac{\sqrt{\alpha}}{\sqrt{\pi(t-\xi)}}\exp\left(\frac{-x^2}{4\alpha(t-\xi)}\right)\mathrm{d}\xi. \tag{13}$$

2.3.2. Distribution of temperature in disk specimen

In order to obtain the temperature distribution in the disk, a semi-infinite solid with a heat source over the circular area $r_i \leqslant r \leqslant r_o$ and $x = 0$, is considered. Note that r_i and r_o are the inner and outer diameter of the tubular specimen, respectively. The temperature rise as a function of time and position can be expressed as

$$T(r,x,t)=\frac{1}{2k\sqrt{\pi\alpha}}\int_0^t \dot{q}(\xi)\frac{\mathrm{d}\xi}{(t-\xi)^{\frac{3}{2}}}\int_{r_i}^{r_o} \mathrm{e}^{-\frac{(r^2+r'^2+x^2)}{4\alpha(t-\xi)}} I_0\left(\frac{rr'}{2\alpha(t-\xi)}\right)r'\mathrm{d}r', \tag{14}$$

where $I_0(z)$ is the modified Bessel function of order zero.

In view of Eq. (14), the temperature distribution at the slip interface (i.e., $x = 0$) can be expressed as

$$T(r,0,t)=\frac{1}{2k\sqrt{\pi\alpha}}\int_0^t \dot{q}(\xi)\frac{\mathrm{d}\xi}{(t-\xi)^{\frac{3}{2}}}\int_{r_i}^{r_o} \mathrm{e}^{-\frac{(r^2+r'^2)}{4\alpha(t-\xi)}} I_0\left(\frac{rr'}{2\alpha(t-\xi)}\right)r'\mathrm{d}r'. \tag{15}$$

In the present experiments the total time duration of interest is less than 1000 μs, r and r' are of the order $20 \sim 30$ mm, and $\alpha \sim 10^{-6}$ m^2/s, such that $\frac{rr'}{2\alpha(t-\xi)} \sim 10^5$. For large z

$$I_0(z)\simeq\frac{\mathrm{e}^z}{\sqrt{2\pi z}}. \tag{16}$$

Next, defining $\lambda = r - r'$, and using Eq. (16) in Eq. (15), the temperature distribution in the bar, $T(r, x = 0, t)$, can be expressed as

$$T(r,0,t)=\frac{1}{2\pi k}\int_0^t \dot{q}(\xi)\frac{\mathrm{d}\xi}{(t-\xi)}\int_{r-r_o}^{r-r_i} \mathrm{e}^{-\frac{\lambda^2}{4\alpha(t-\xi)}}\sqrt{1-\frac{\lambda}{r}}\mathrm{d}\lambda. \tag{17}$$

Since the thickness of tubular specimen is small compared to the radius of tubular specimen, $\sqrt{1-\frac{\lambda}{r}} \simeq 1$. In view of this, Eq. (17) becomes

$$T(r,0,t)\doteq\frac{1}{2\pi k}\int_0^t \dot{q}(\xi)\frac{\mathrm{d}\xi}{(t-\xi)}\int_{r-r_o}^{r-r_i} \mathrm{e}^{-\frac{\lambda^2}{4\alpha(t-\xi)}}\mathrm{d}\lambda. \tag{18}$$

Next, by expressing the integral $\int_{-a_1}^{a_2} \mathrm{e}^{\left(-\frac{x^2}{a}\right)}\mathrm{d}x$ as a sum of the error functions, i.e., $\int_{-a_1}^{a_2} \mathrm{e}^{\left(\frac{-x^2}{a}\right)}\mathrm{d}x = \frac{\sqrt{a\pi}}{2}\left(erf\left(\frac{a_1}{\sqrt{a}}\right)+erf\left(\frac{a_2}{\sqrt{a}}\right)\right)$, Eq. (18) can be written as

$$T(r,0,t)=\frac{\sqrt{\alpha}}{2k\sqrt{\pi}}\int_0^t \frac{\dot{q}(\xi)}{\sqrt{t-\xi}}\left[erf\left(\frac{r_o-r}{\sqrt{4\alpha(t-\xi)}}\right)+erf\left(\frac{r-r_i}{\sqrt{4\alpha(t-\xi)}}\right)\right]\mathrm{d}\xi. \tag{19}$$

In the present experiments $r_i = 22$ mm, $r_o = 25$ mm, and thus for $r_i + 0.1$ mm $< r < r_o - 0.1$ mm, we can approximate

$$erf\left(\frac{r_o-r}{\sqrt{4\alpha(t-\xi)}}\right)=erf\left(\frac{r-r_i}{\sqrt{4\alpha(t-\xi)}}\right)\simeq 1. \tag{20}$$

In view of this, for the region bounded by the circular area $r_i \leqslant r \leqslant r_o$, the temperature $T(x = 0, t)$ can be expressed as

$$T(0,t)=\frac{1}{k}\int_0^t \dot{q}(\xi)\frac{\sqrt{\alpha}}{\sqrt{\pi(t-\xi)}}\mathrm{d}\xi. \tag{21}$$

2.3.3. Temperature rise at the slip interface

In order to calculate the temperature distribution in the tribo-pair materials, an estimate for the heat source $\dot{q}(t)$ is required. Using the experimentally measured friction stress, τ, and the slip velocity, V^{slip}, the frictional power at the slip interface can be written as

$$\dot{q}_{\text{tubular}}(t) = \beta\tau(t)V^{\text{slip}}(t), \tag{22}$$

$$\dot{q}_{\text{disk}}(t) = (1-\beta)\tau(t)V^{\text{slip}}(t), \tag{23}$$

where, β is the factor that governs the partitioning of heat in the tribo-pair materials.

The factor β can be estimated by equating the temperatures at the tribo-pair interface to yield

$$\beta = \frac{k_{\text{tubular}}\sqrt{\alpha_{\text{disk}}}}{k_{\text{tubular}}\sqrt{\alpha_{\text{disk}}} + k_{\text{disk}}\sqrt{\alpha_{\text{tubular}}}}. \tag{24}$$

In the present study, for glass on glass slip $\beta = 0.5$, and the temperature rise at the slip interface can determined by

$$T(0,t) = \frac{1}{2}\frac{\sqrt{\alpha}}{k\sqrt{\pi}}\int_0^t \tau(\xi)V^{\text{slip}}(\xi)\frac{1}{\sqrt{(t-\xi)}}\mathrm{d}\xi. \tag{25}$$

3. Experimental results

Using the modified torsional Kolsky bar, a series of experiments was conducted to investigate the frictional resistance of quartz on quartz at co-seismic slip rates. The quartz specimen are from American Precision Glass Corp. (Duryea, PA), and the quartz material is 100% SiO_2. Table 2 summarizes the two experiments conducted in this series. The tribo-pair comprises of a thin-walled tubular quartz specimen and a quartz disk. The RMS surface roughness of the quartz tube was 220 nm while the RMS surface roughness of the quartz disk was 3 nm. The outer and inner diameters for the tubular quartz specimen were 25 and 22 mm, respectively. Experiment Q01 was conducted at an input torque of 38.5 Nm and a normal stress of 66.8 MPa, while experiment Q02 was conducted at an input torque of 66.3 Nm and a normal stress of 72.2 MPa. The objective of the two experiments was to keep the normal stress nearly the same for the two experiments but vary the input torque. By increasing the input torque in experiment Q02, a higher slip speed is expected in Q02 when compared to Q01 at nearly the same normal stress. The higher slip speeds are expected to generate much higher flash temperatures, and thus a lower coefficient of friction due to thermal softening.

The experimental results for Q01 are shown in Figs. 5–9. Fig. 5 shows the experimentally measured torque at the strain gage location A for Q01. The input torsional pulse has a magnitude of 38.5 Nm and a pulse duration of 1000 μs. Fig. 6 shows the history of normal stress, shear-stress and slip velocity as a function of time after the arrival of the shear loading pulse at the tribo-pair interface. Fig. 7 shows the coefficient of kinetic friction, interfacial normal stress and the slip velocity as a function of slip distance. These quantities were calculated by using the strain gage profiles and the elastic 1-D wave theory presented in Section 2. Fig. 8 shows the "bulk" temperature rise at the tribo-pair interface estimated by using the transient heat conduction Eq. (25). Fig. 9 shows sequential images of tribo-pair specimen obtained by using the high-speed camera. The inter-frame time for the images was 50 μs.

From the experimental results shown in Fig. 6, it is to be noted that the interfacial normal stress maintains a steady-state level of approximately 67 MPa up to 250 μs, and then starts to decrease gradually. The drop in normal stress is understood to coincide with the initiation of failure in the tubular quartz specimen, as observed from the high-speed camera images shown in Fig. 9. The initiation of micro-cracking can be observed from the third frame of the high-speed camera images ($t \sim 250$ μs), which corresponds to the drop in normal stress in Fig. 6. The interfacial shear stress increases from zero to a steady-state level of approximately 15 MPa, and then decreases to zero with the accumulation of failure in the tubular specimen. The coefficient of kinetic friction has a maximum of 0.23, and then decreases to essentially zero as the tube wall cannot support any shear. The average interfacial slip velocity during the window time is ~2 m/s. The corresponding accumulated slip distance is 0.35 mm. The maximum temperature rise at the tribo-pair interface, as shown in Fig. 8, is 140 °C and is not high enough for macroscopic melting to occur at the slip interface – so the much lower coefficient of friction ($\mu \sim 0.2$) when compared to those obtained by Byerlee (1978) and Dieterich (1978) at quasi-static slip rates ($\leqslant$1 mm/s, $\mu \sim 0.6$ to 0.85) is understood to be attributed to thermal weakening induced by the high flash temperatures at the asperity contacts.

The experimental results for Q02 are shown in Figs. 10–14. Fig. 10 shows the experimentally measured torque at the strain gage location A for Q02. The input torsional pulse has a magnitude of 66.3 Nm and a pulse duration of 1000 μs. This level of the input torque is almost twice as large as that employed in experiment Q01. Fig. 11 shows the history of normal stress, the interfacial shear stress and slip velocity. Fig. 12 show the corresponding coefficient of kinetic friction, normal stress and the slip velocity as a function of slip distance. Fig. 13 shows the "bulk" temperature rise at the tribo-pair interface. Fig. 14 shows sequential images of tribo-pair specimens from the high-speed camera with an inter-frame time of 50 μs.

Table 2
Summary of modified torsional Kolsky bar friction experiments conducted on quartz

SHOT #	Input torque (Nm)	Normal stress σ, MPa	Highest shear stress (MPa)	Highest coefficient of kinetic friction	Roughness of quartz Tube (nm)	Roughness of quartz disk (nm)
Q01	38.5	66.8	14.5	0.22	220	3
Q02	66.3	72.2	14.1	0.20	220	3

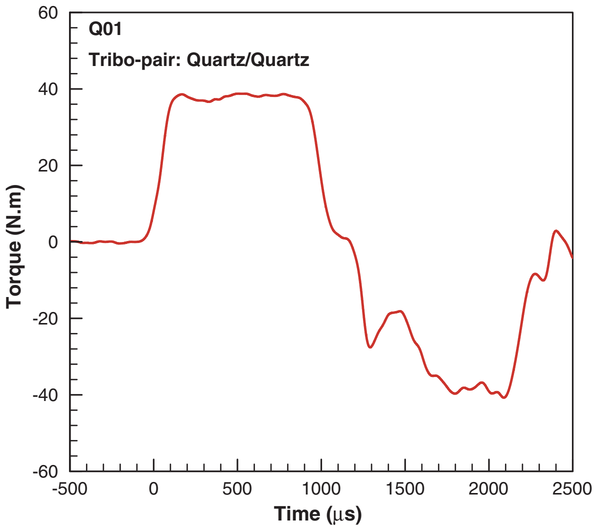

Fig. 5. Measured torque at the strain gage location A for experiment Q01.

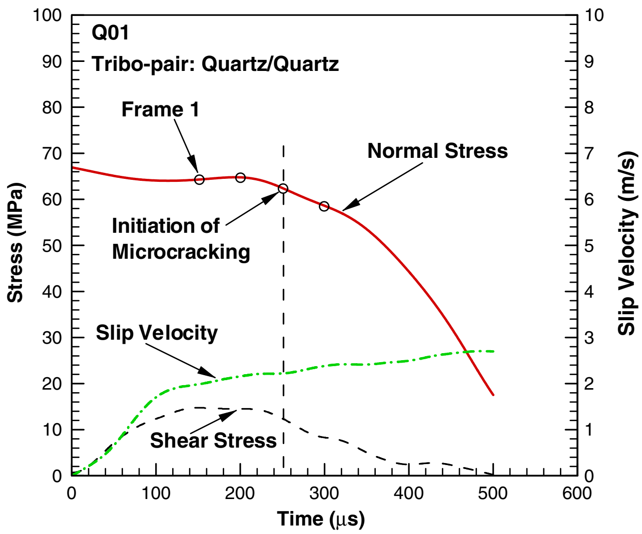

Fig. 6. History of interfacial normal stress, friction (shear) stress and slip velocity for experiment Q01.

As was the case in experiment Q01, the interfacial normal stress maintains a steady-state level of approximately 72 MPa up to 150 μs, after which it starts to fall. The drop in normal relatively higher stress can be attributed to the initiation and propagation of damage in the tubular quartz specimen. The initiation of micro-cracking can be seen from the third frame onwards in the high-speed camera images, which implies that the initiation of microcracking occurs between 100 and 150 μs (second and the third frame in Fig. 11). The interfacial shear stress increases to a steady-state level of approximately 14 MPa and then decrease to zero with the drop in normal stress. Due to micro-cracking and fracture of tubular quartz specimen, the useful window time for the experiment is only about 100 μs. The coefficient of kinetic friction has a maximum level of 0.20 (Fig. 12) during this window time. The average interfacial slip velocity is ~4 m/s. The corresponding accumulated slip distance is approximately 0.4 mm. The resulting coefficient of kinetic friction is $\mu \sim 0.2$, which is lower than that attained in experiment Q01 ($\mu \sim 0.23$). This can be attributed to the higher interfacial slip velocities attained in this experiment. Note that in this experiment (Q02) a higher slip velocity was expected since a higher level of input torque was employed.

In experiments Q01 and Q02, due to micro-cracking and fracture of the tubular quartz specimen, the accumulated slip distance was limited to be <0.5 mm. These relatively small slip distances limit the time for observation of the slip phenomena. In order to extend the study of interfacial slip to much larger slip distances, the thin-walled tubular quartz specimens were replaced by thin-walled aluminum tubes with a thin-film of soda-lime glass (thickness ~1 μm) deposited on one of the

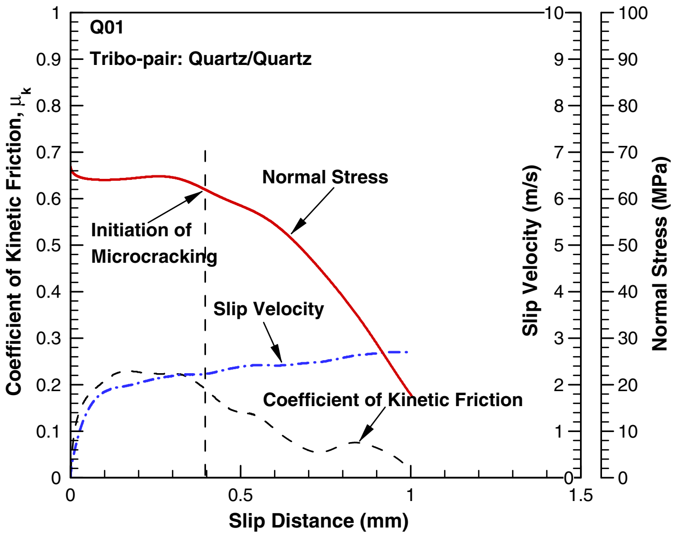

Fig. 7. Interfacial normal stress, slip velocity and coefficient of kinetic friction as a function of interfacial slip distance for experiment Q01.

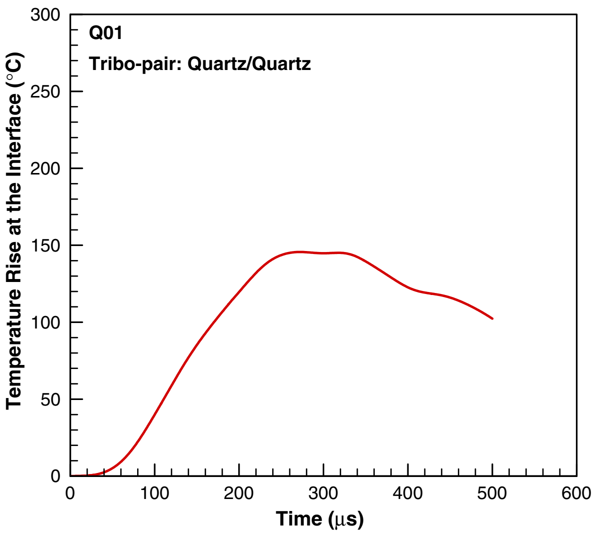

Fig. 8. Estimated temperature rise at tribo-pair interface for experiment Q01.

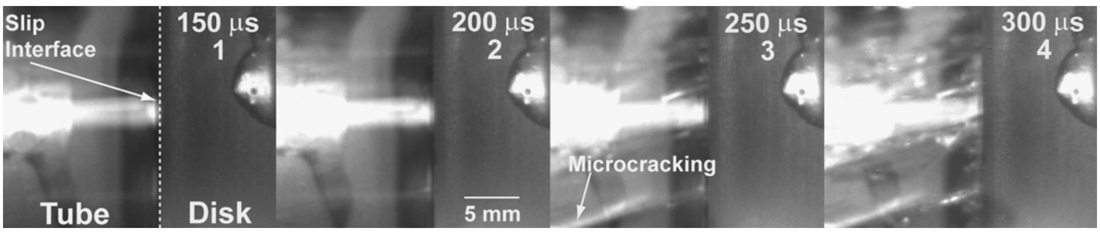

Fig. 9. High-speed camera images for experiment Q01. Micro-cracking in the glass tubular specimen can be seen to develop from Frame 3 onwards.

faces. Consequently, the quartz disk is replaced by a soda-lime glass disk specimen. The thin soda-lime glass film is expected to prevent catastrophic failure of the specimen at relatively small slip distances present in the relatively brittle glass tubular specimens used in the first series of experiments.

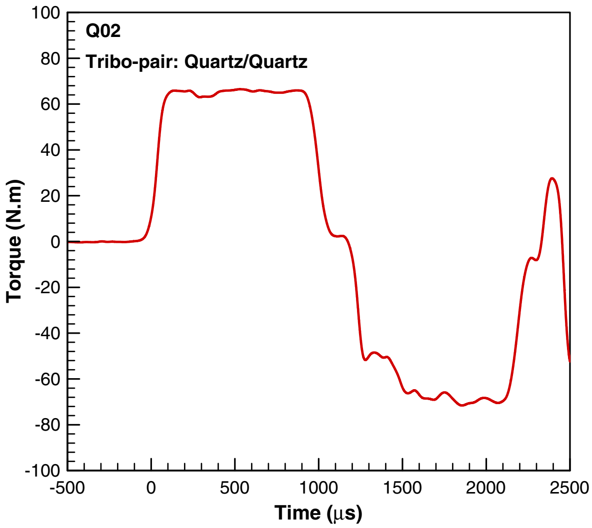

Fig. 10. Measured torque at the strain gage location A for experiment Q02.

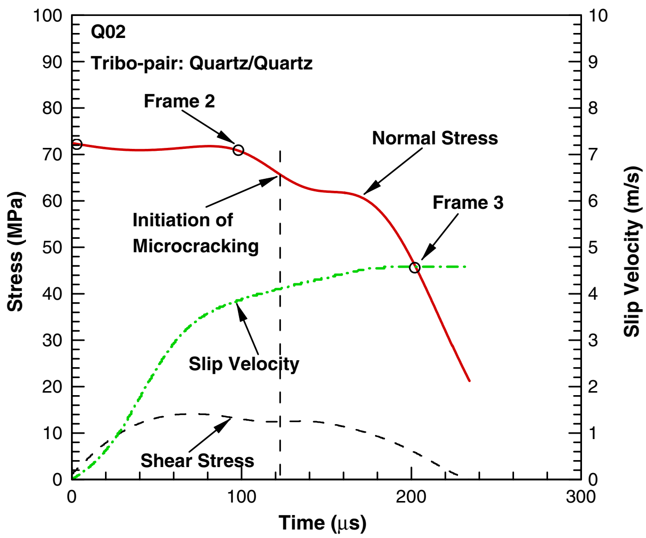

Fig. 11. History of interfacial normal stress, friction (shear) stress and slip velocity for experiment Q02.

Table 3 summarizes the six experiments conducted on soda-lime glass tribo-pair. The outer and inner diameters for the aluminum tubular specimens were 25.4 and 21.6 mm, respectively. For experiments G01 to G03 the interfacial normal stress was maintained at ~70 MPa, but the input torque was varied from 44.8 to 81.5 Nm. For experiments G04 to G06 the normal stress was kept at ~40 MPa and the input torque was varied from 43.2 to 68.8 Nm. In all the six experiments the RMS surface roughness of the soda lime glass coating was maintained at ~18 nm while the RMS surface roughness of the soda lime glass disk was kept at 4 nm.

The experimental results for G02 are shown in Figs. 15 and 16. Fig. 15 shows the measured torque at the strain gage location A. The input torsional pulse has a magnitude of 53.1 N.m and a pulse duration of 1000 μs. Fig. 16 shows the coefficient of kinetic friction,the interfacial slip velocity and the "bulk" temperature rise at the interface as a function of the slip distance. Unlike in the first series of experiments (i.e., Q01 and Q02), the interfacial normal stress in experiment GO2 is nearly constant for the entire duration of the experiment. The interfacial slip velocity increases from zero to approximately 2.5 m/s and then oscillates in the vicinity of this level. As a result, the accumulated slip distance is around 2.2 mm, which is much larger when compared to that obtained in experiments Q01 and Q02. The coefficient of kinetic friction during the early part of slip has an average value of 0.29; with an accumulation of slip the coefficient of kinetic friction decreases from 0.29 to 0.21, indicating slip weakening, and then increases to 0.27 indicating slip strengthening at the slip

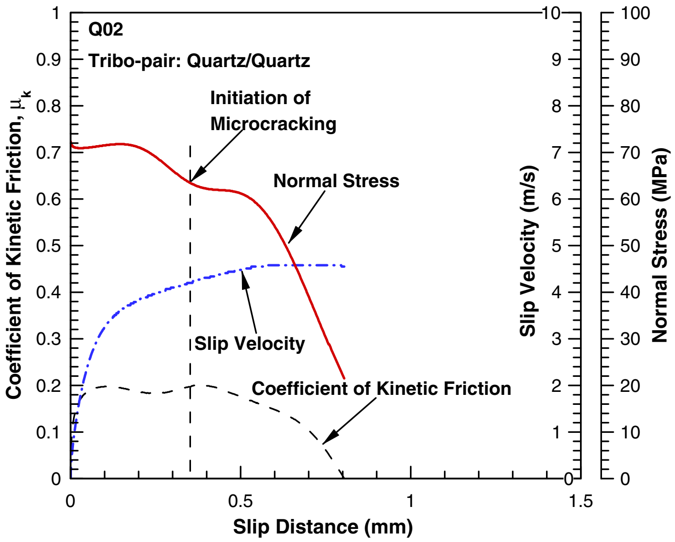

Fig. 12. Interfacial normal stress, slip velocity and coefficient of kinetic friction as a function of interfacial slip distance for experiment Q02.

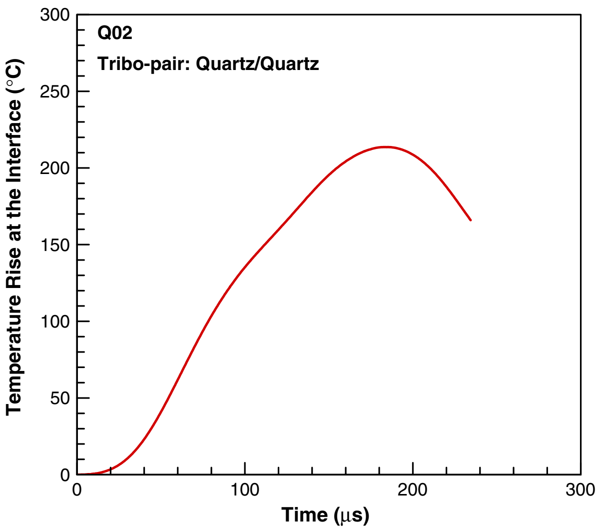

Fig. 13. Estimated temperature rise at tribo-pair interface for experiment Q02.

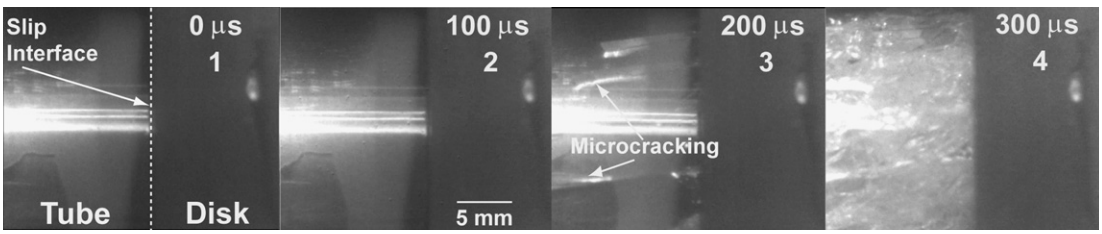

Fig. 14. High-speed camera images for Q02. Again micro-cracking in the tubular quartz specimen can be seen to develop from Frame 3 onwards.

interface. It is to be noted that we do not observe seizure at the slip interface, and during the slip strengthening phase the coefficient of friction increases to its local maximum and then decreases with slip. This is seen as oscillations in the coefficient of friction profile in Fig. 16 after the slip strengthening phase. The "bulk" temperature rise at the tribo-pair interface

Table 3
Summary of modified torsional Kolsky bar friction experiments conducted on soda-lime glass

SHOT #	Input torque (Nm)	Normal Stress σ, MPa	Highest shear stress (MPa)	Highest coefficient of kinetic friction	Roughness of glass film (nm)	Roughness of glass disk (nm)
G01	81.5	76.1	15.2	0.20	18	4
G02	53.1	69.2	20.8	0.30	18	4
G03	44.8	71.9	22.3	0.31	18	4
G04	68.8	44.5	12.5	0.28	18	4
G05	60.1	38.0	11.8	0.31	18	4
G06	43.2	37.8	11.7	0.31	18	4

(shown in Fig. 16) is 500 °C, and is not high enough for macroscopic melting. However, the much lower friction coefficients ($\mu \sim 0.29$ to 0.21) can be attributed to thermal weakening induced by the high flash temperatures at the asperity contacts.

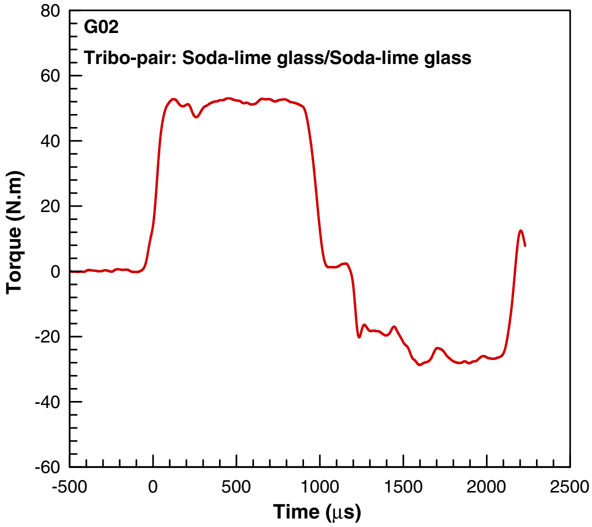

Fig. 15. Measured torque at the strain gage location A for experiment G02.

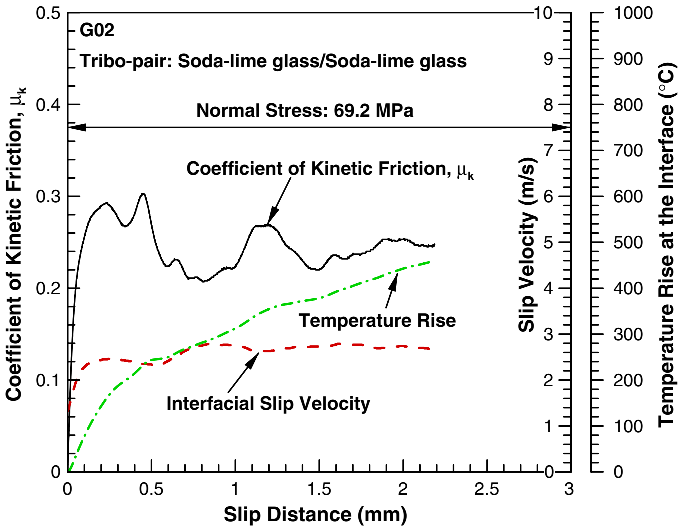

Fig. 16. Slip velocity and coefficient of kinetic friction as a function of interfacial slip distance for experiment G02.

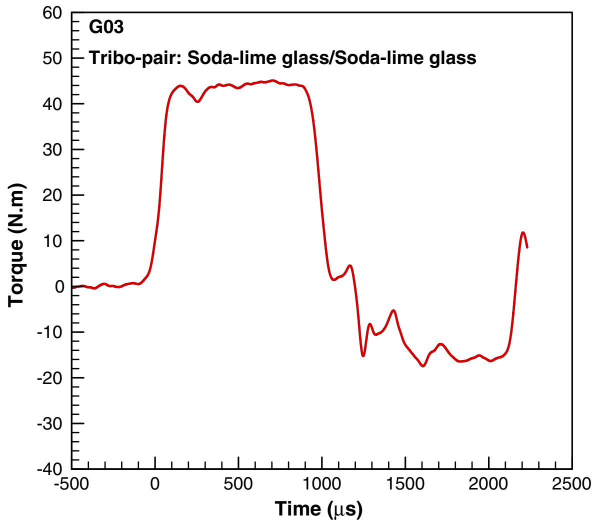

Fig. 17. Measured torque at the strain gage location A for experiment G03.

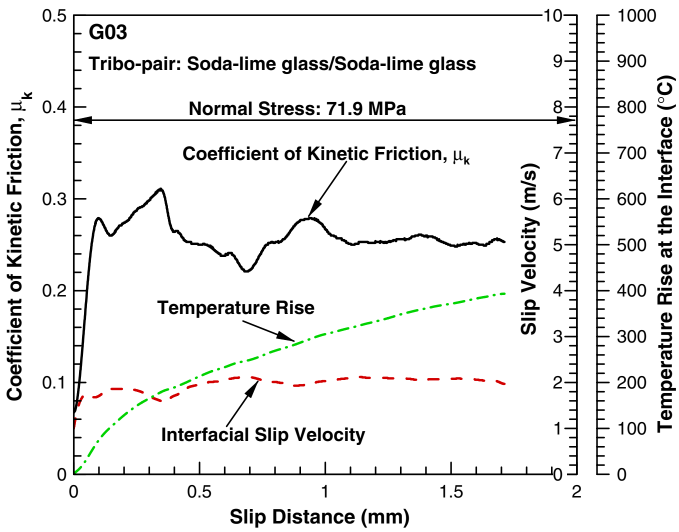

Fig. 18. Slip velocity and coefficient of kinetic friction as a function of interfacial slip distance for experiment G03.

The experimental results for G03 are shown in Figs. 17 and 18. The normal stress for experiment G03 is 71.9 MPa, which is similar to the normal stress levels employed in experiments GO1 and G02. However, the input torsional pulse has a magnitude of 44.8 Nm (with a pulse duration of 1000 μs), which is similar to that employed in experiment G02 but much lower when compared to experiment G01. The interfacial slip velocity reaches a maximum of 2.0 m/s and then oscillates in the vicinity of this level. The total accumulated slip distance is around 1.7 mm. The coefficient of kinetic friction shows similar behavior as that observed in experiment G02 – during the early part of slip has an average value of 0.28, decreases to 0.22 with accumulation of slip indicating slip weakening, and then increases again to 0.27 indicating slip strengthening followed the slip weakening. The maximum bulk temperature rise at the tribo-pair interface is again much lower than the melt point of the soda-lime glass.

The experimental results for G06 are shown in Figs. 19 and 20. The experiment was conducted at a normal stress of 40 MPa, which is lower than that employed in experiments G01 to G03 (~70 MPa). The input torsional pulse has a magnitude of 43.2 Nm and a pulse duration of 1000 μs; the interfacial slip velocity rises from zero to approximately 2.3 m/s and then oscillates at this level. The accumulated slip distance is ~1.9 mm. The coefficient of kinetic friction during the early part of slip has an average value of 0.31, decreases to 0.15 with the accumulation of slip and then increases again to 0.26 indicating slip strengthening following the initial slip weakening. The bulk temperature rise at the tribo-pair interface was 200 °C, which is much lower than the melt point of the soda-lime glass.

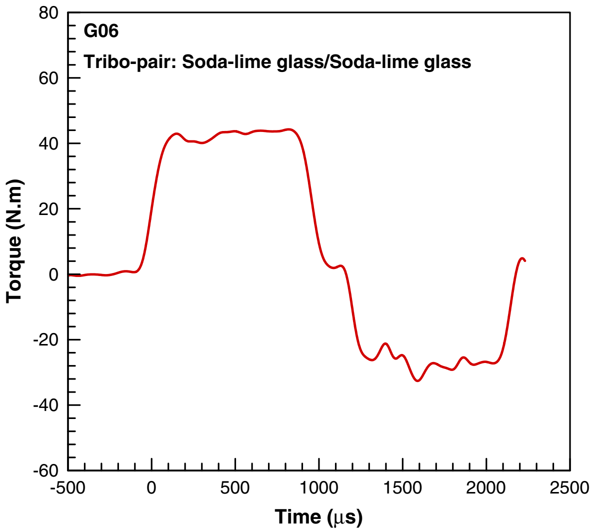

Fig. 19. Measured torque at the strain gage location A for experiment G06.

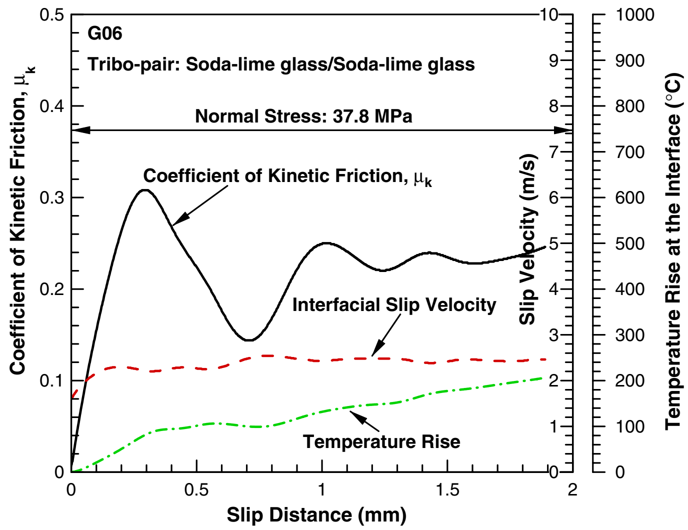

Fig. 20. Slip velocity and coefficient of kinetic friction as a function of interfacial slip distance for experiment G06.

Fig. 21 summarizes the highest coefficient of kinetic friction versus interfacial slip velocity obtained from all six experiments conducted on the soda lime glass/soda lime glass tribo-pair. It is interesting to note that the highest coefficient of kinetic friction in each experiment decreases with the increasing slip velocity. Moreover, the interfacial normal stress has negligible effect on the highest coefficient of kinetic friction.

Figs. 22 and 23 show SEM micrographs of sliding surfaces of the pre-test and post-test soda-lime glass specimens obtained from experiment G01; slip direction is from the bottom to the top in the post-test specimens. It is to be noted that during the slip-weakening phase of a typical slip event, even though the bulk temperature rise is small the flash temperatures at the asperity contacts are expected to approach the near-melt temperatures of soda-lime glass. As slip precedes these soft near-melt asperity junctions continuously increase in size by local plastic flow leading to an increase in effective area of contact, and thus to healing and strengthening of the slip interface. Strengthening of the interface is also aided by an increase in shear-strength of the plastically deformed asperity junctions as they are rapidly quenched by the surrounding lower temperature material. Sliding wear tracks including smearing of the highly deformed glass can easily be identified on the slip interface of post-test specimens, indicating localized plastic flow due to thermal softening at the slip surfaces. These micrographs provide further evidence that thermal softening and subsequent plastic flow may be responsible for the observed initial slip weakening followed by slip strengthening (i.e., healing) at the slip interface.

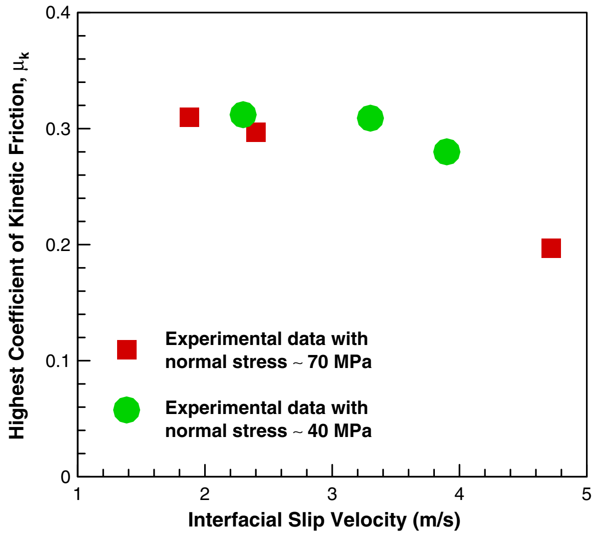

Fig. 21. Highest coefficient of kinetic friction versus interfacial slip velocity obtained from experiments conducted on the soda-lime glass/soda-lime glass tribo-pair.

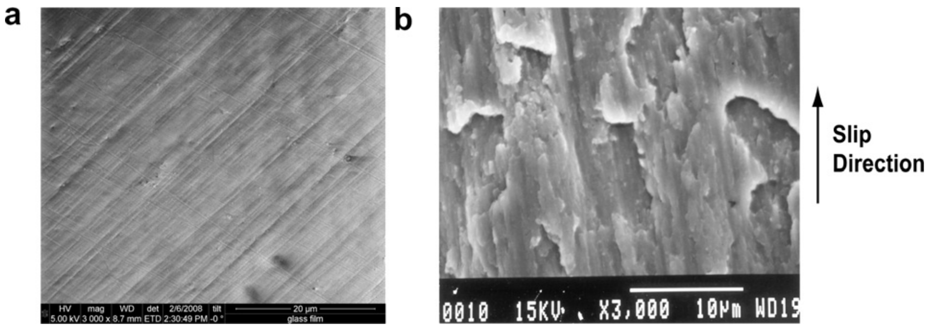

Fig. 22. SEM micrographs for sliding surface of soda-lime glass thin film obtained from G01. (a) Pre-test specimen showing polishing marks that run diagonally; (b) Post-test specimen showing plastic flow including asperity ploughing along the slip direction.

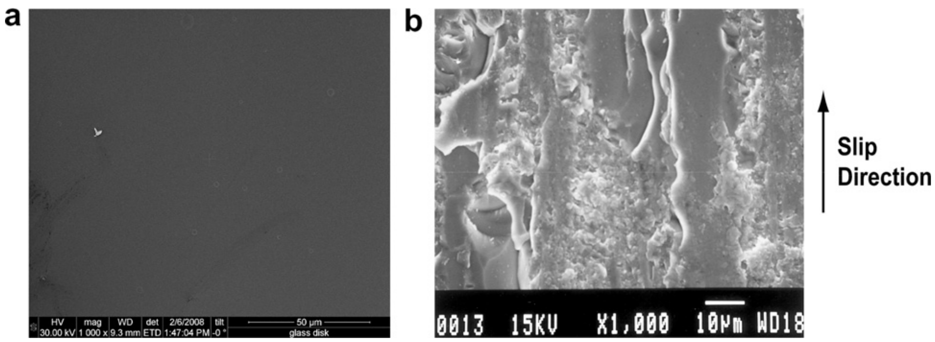

Fig. 23. SEM micrographs for sliding surface of soda-lime glass disk specimen obtained from G01. (a) Pre-test. (b) Post-test specimen showing plastic flow in the direction of slip.

4. Summary and discussions

Recent theoretical and laboratory studies on frictional properties of geo-materials at coseismic slip rates suggest relevant weakening processes in large crustal events to be thermal in origin. In this regard, field observations of mature crustal faults indicate that slip in individual events occurs primarily within a thin shear zone, <1–5 mm, within a finely granulated, ultracataclastic fault core. As perhaps the best characterized case, a thin "principal slip surface" (PSS) was identified along an exposure of the Punchbowl fault, which was exhumed from 2 to 4 km depth and had accommodated ∼44 km of slip (Chester and Chester, 1998; Chester et al., 1999). Subsequent studies (Chester et al., 2004, 2005) of thin sections of samples from the fault core showed that the nominal thickness of the shear zone, as revealed by uniform birefringence in crossed polarizers due to preferred orientation of the sheared minerals within it, varied from 0.6 to 1.1 mm at different locations along the sample. However, within this ∼1 mm thick "nominal" shear zone, most of the shearing seemed to have been accommodated within a zone of extreme shear localization with an apparent thickness of 100–300 μm. The evidence for narrowness of the shear zone, where frictional work is dissipated, suggests that unless we appeal to some mechanism to rapidly diminish fault strength as slip accumulates, the temperature rise in the shear zone will far exceed those for the onset of melting. However, evidence of melting in the form of pseudotachylytes has been rare. Where pseudotachylytes are found and attributable to tectonic faulting, the inferred depths are generally towards the lower reaches of the seismogenic zone (Sibson, 1975, 1980). These observations provide compelling evidence that fault strength cannot remain constant during earthquake slip, at least at a static friction coefficient of ∼0.6 or higher (Byerlee, 1978; Dieterich, 1978; Dieterich and Kilgore, 1996a), but must weaken substantially to explain the apparent absence of melt.

In the present study, a modified torsional Kolsky bar is used to better understand frictional resistance in rock-analog materials (quartz and soda-lime glass) at relevant normal pressures (30–80 MPa) and co-seismic slip rates. The results of the experiments (both for soda-lime glass and quartz) indicate the coefficient of kinetic friction values to be 0.2 to 0.3 which are much lower than those obtained by Byerlee (1978) and Dieterich (1978) at quasi-static slip rates ($\leqslant$1 mm/s, $\mu \sim 0.6$ to 0.85). Moreover, in all experiments the coefficient of kinetic friction shows initial slip weakening, followed by slip strengthening at the larger slip distances. Similar slip behavior has also been observed in the pressure-shear experiments in soda-lime glass (Yuan and Prakash, 2008) at slip speeds in several m/s range and by Goldsby and Tullis (2002), at slip speeds in the mm/s range.

Recent measurements of contact area and contact indentation strength in transparent materials, such as quartz, by light scattering (Dieterich and Kilgore, 1994, 1996b), confirmed earlier suggestions by Boitnott et al. (1992) that the shear strength of the asperity junctions is very high (estimated to be of order 10% of the shear modulus G) in typical rock systems, and thus when forced to shear, they generate intense but highly localized heating during their life time. The local shear strength of the asperity contact presumably degrades continuously with increasing flash temperature. An elementary model considering flash heating at asperity contacts had been proposed recently by Rice (2006). The model considers contacts of uniform size L, and hence life-time L/V, where L is the slip needed to renew the asperity contact population, and V is slip rate; and assumes that their shear strength remains at the room temperature value until temperature has reached a critical value above which the weakened shear strength is assumed to has a negligibly small compared to its room temperature value. The temperature rise of the asperities is estimated from a simple one-dimensional transient heat conduction equation. Based on this model a critical velocity of V_{crit} = 0.12 m/s can been estimated to be onset of severe thermal weakening at asperity contacts in glass and other geo-materials for L = 5 μm and a critical shear strength of ∼3.0 GPa, which is approximately 10% of the shear modulus of soda-lime glass (Dieterich and Kilgore, 1994, 1996b). The results of the present study are indeed consistent with such an expected reduction in friction stress, and suggest a friction coefficient in the range of 0.2 to 0.3 at seismic slip rates of ∼1 m/s in geo-materials.

Acknowledgements

This research was supported by the Southern California Earthquake Center. SCEC is funded by NSF Cooperative Agreement EAR-0529922 and USGS Cooperative Agreement 07HQAG0008. The SCEC contribution number for this paper is 1150. The authors would also like to acknowledge the Case Graduate Student Prime Fellowship, and the NSF Major Research Instrumentation Awards CMS-0079458 and CMMI-0521364 for the acquisition of the DRS Hadland ultra-high-speed digital camera and the FEI FE NanoSEM 600 used for microscopy in the present study.

References

Andrews, D.J., 2002. A fault constitutive relation accounting for thermal pressurization of pore fluid. Journal of Geophysical Research 107 (B12), 2363. doi: 2310.1029/ 2002JB001942, ESE 001915-001941–001915-001948.

Archard, J.F., 1958. The temperature of rubbing surfaces. Wear 2, 438–455.

Ashby, M.F., Abulawi, J., Kong, H.S., 1991. Temperature maps for frictional heating in dry sliding. Tribology Transactions 34 (4), 577–587.

Barber, J.R., 1976. Some thermoelastic contact problems involving frictional heating. The Quarterly Journal of Mechanics and Applied Mathematics 29, 1–13.

Blanpied, M.L., Tullis, T.E., Weeks, J.D., 1998. Effects of slip, slip rate, and shear heating on the friction of granite. Journal of Geophysical Research-Solid Earth 103 (B1), 489–511.

Boitnott, G.N., Biegel, R.L., Scholz, C.H., Yoshioka, N., Wang, W., 1992. Micromechanics of rock friction 2: quantitative modeling of initial friction with contact theory. Journal of Geophysics Research 97, 8965–8978.

Bowden, F.P., Thomas, P.H., 1954. The surface temperature of sliding solids. Proceedings of Royal Society of London A 223, 29–36.

Byerlee, J.D., 1978. Friction of rocks. Pure and Applied Geophysics 116, 615–626.

Chester, F.M., Chester, J.S., 1998. Ultracataclasite structure and friction processes of the Punchbowl fault, San Andreas system, California. Tectonophysics 295, 199–221.

Chester, F.M., Kirschner, D.L., Chester, J.S., 1999. Extreme localization of slip during earthquake rupture – field evidence from the Punchbowl and San Gabriel faults, San Andreas system, California. EOS Transactions of AGU 80, F689.

Chester, J.S., Chester, F.M., Kronenberg, A.K., 2004. Fracture surface energy of mature fault zones from structural observations of the Punchbowl fault, California. EOS Transactions on American Geophysics 85 (17). Union, Spring Meeting Suppl.
Chester, J.S., Chester, F.M., Kronenberg, A.K., 2005. Fracture surface energy of the Punchbowl fault, San Andreas system. Nature 437, 133–135.
Di Toro, G., Goldsby, D.L., Tullis, T.E., 2004. Friction falls towards zero in quartz rock as slip velocity approaches seismic rates. Nature 427 (6973), 436–439.
Dieterich, J.H., 1978. Time dependent friction and mechanics of stick-slip. Pure and Applied Geophysics 116, 668–675.
Dieterich, J.H., 1979. Modeling of rock friction: I. Experimental results and constitutive equations. Journal of Geophysical Research 84 (B5), 2161–2168.
Dieterich, J.H., 1981. In: Carter, N.L., Friedman, M., Logan, J.M., Stearns, D.W. (Eds.), Constitutive Properties of Faults with Simulated Gouge, vol. 24. American Geophysical Union, Washington, DC, pp. 103–120.
Dieterich, J.H., Kilgore, B.D., 1994. Direct observation of frictional contacts – new insights for state-dependent properties. Pure and Applied Geophysics 143 (1–3), 283–302.
Dieterich, J.H., Kilgore, B., 1996a. Implications of fault constitutive properties for earthquake prediction. Proceedings of the National Academy of Sciences of the United States of America 93 (9), 3787–3794.
Dieterich, J.H., Kilgore, B.D., 1996b. Imaging surface contacts: power law contact distributions and contact stresses in quartz, calcite, glass and acrylic plastic. Tectonophysics 256 (1–4), 219–239.
Goldsby, D., Tullis, T.E., 2002. Low frictional strength of quartz rocks at sub-seismic slip rates. Geophysical Research Letters 29 (17), 1844.
Heaton, T.H., 1990. Evidence for and implications of self-healing pulses of slip in earthquake rupture. Physics of the Earth and Planetary Interiors 64, 1–20.
Hirose, T., Shimamoto, T., 2005. Growth of molten zone as a mechanism of slip weakening of simulated faults in gabbro during frictional melting. Journal of Geophysical Research-Solid Earth 110 (B5).
Irfan, M.A., Prakash, V., 1994. Contact temperatures during sliding in pressure shear impact. In: Proceedings Society of Experimental Mechanics Conference, Baltimore, MD, pp. 173–182.
Kuhlmann-Wilsdorf, D., 1985. Flash temperatures due to friction and joule heat at asperity contact. Wear 105, 187–198.
Lachenbruch, A.H., 1980. Frictional heating, fluid pressure, and the resistance to fault motion. Journal of Geophysical Research 85 (B11), 6097–6122.
Lee, T.C., Delaney, P.T., 1987. Frictional heating and pore pressure rise due to a fault slip. Geophysical Journal of Royal Astronomical Society 88 (3), 569–591.
Marone, C., 1998. Laboratory-derived friction laws and their application to seismic faulting. Annual Review Earth and Planetary Science 26, 643–696.
Mase, C.W., Smith, L., 1985. Pore–fluid pressures and frictional heating on a fault surface. Pure and Applied Geophysics 122, 583–607.
Mase, C.W., Smith, L., 1987. Effects of frictional heating on the thermal, hydrologic, and mechanical response of a fault. Journal of Geophysical Research 92 (B7), 6249–6272.
Mizoguchi, K., Hirose, T., Shimamoto, T., Fukuyama, E., 2006. Moisture-related weakening and strengthening of a fault activated at seismic slip rates. Geophysical Research Letters 33 (16).
Noda, H., Shimamoto, T., 2005. Thermal pressurization and slip-weakening distance of a fault: An example of the Hanaore fault, southwest Japan. Bulletin of the Seismological Society of America 95 (4), 1224–1233.
O'Hara, K., Mizoguchi, K., Shimamoto, T., Hower, J.C., 2006. Experimental frictional heating of coal gouge at seismic slip rates: evidence for devolatilization and thermal pressurization of gouge fluids. Tectonophysics 424 (1–2), 109–118.
Rajagopalan, S., Irfan, M.A., Prakash, V., 1999. Novel experimental techniques for investigating time resolved high speed friction. Wear 225–229, 1222–1237.
Rajagopalan, S., Prakash, V., 1999. A modified torsional Kolsky bar for investigating dynamic friction. Experimental Mechanics 39 (4), 295–303.
Rempel, A.W., Rice, J.R., 2006. Thermal pressurization and onset of melting in fault zones. Journal of Geophysical Research-Solid Earth 111 (B9).
Rice, J.R., Ruina, A., 1983. Stability of steady frictional sliding. Journal of Applied Mechanics 50, 343–349.
Rice, J.R., 2006. Heating and weakening of faults during earthquake slip. Journal of Geophysical Research-Solid Earth 111 (B5).
Rudnicki, J.W., Rice, J.R., 2006. Effective normal stress alteration due to pore pressure changes induced by dynamic slip propagation on a plane between dissimilar materials. Journal of Geophysical Research-Solid Earth 111 (B10).
Ruina, A., 1983. Slip stability and state variable friction laws. Journal of Geophysical Research 88 (B12), 10359–10370.
Scholz, C.H., Molnar, P., Johnson, T., 1972. Detailed studies of frictional sliding of granite and implications for the earthquake mechanism. Journal of Geophysical Research 77 (32), 6392–6406.
Scholz, C.H., 1998. Earthquakes and friction laws. Nature 243, 37–42.
Segall, P., Rice, J.R., 2006. Does shear heating of pore fluid contribute to earthquake nucleation? Journal of Geophysical Research-Solid Earth 111 (B9).
Sibson, R.H., 1973. Interaction between temperature and pore-fluid pressure during earthquake faulting – a mechanism for partial or total stress relief. Nature 243, 66–68.
Sibson, R.H., 1975. Generation of pseudotachylyte by Ancient Seismic Faulting. Geophysical Journal of Royal Astronomical Society 43, 775–794.
Sibson, R.H., 1980. Power dissipation and stress levels on faults in the upper crust. Journal of Geophysical Research 85, 6239–6247.
Sulem, J., Vardoulakis, I., Ouffroukh, H., Perdikatsis, V., 2005. Thermo-poro-mechanical properties of the Aigion fault clayey gouge – application to the analysis of shear heating and fluid pressurization. Soils and Foundations 45 (2), 97–108.
Tsutsumi, A., Shimamoto, T., 1997. High-velocity frictional properties of gabbro. Geophysical Research Letters 24, 699–702.
Tullis, T.E., 1994. Predicting earthquakes and the mechanics of fault slip. Geotimes 39 (7), 19–21.
Weeks, J.D., Beeler, N.M., Tullis, T.E., 1991. Frictional behavior; glass is like a rock. pp. 457–458.
Wibberley, C.A.J., 2002. Hydraulic diffusivity of fault gouge zones and implications for thermal pressurization during seismic slip. Earth Planets Space 54, 1153–1171.
Wibberley, C.A.J., Shimamoto, T., 2005. Earthquake slip weakening and asperities explained by thermal pressurization. Nature 436 (7051), 689–692.
Yuan, F., Prakash, V., 2008. Slip weakening in rocks and analog materials at coseismic slip rates. Journal of the Mechanics and Physics of Solids 56, 542–560.